Journal of Magnetism and Magnetic Materials 451 (2018) 532–539

Contents lists available at ScienceDirect

Journal of Magnetism and Magnetic Materials

journal homepage: www.elsevier.com/locate/jmmm

Research articles

High efficiency spin-valve and spin-filter in a doped rhombic graphene quantum dot device

P.V. Silva [a,b], A. Saraiva-Souza [b,*], D.W. Maia [b], F.M. Souza [c], A.G. Souza Filho [a], V. Meunier [d], E.C. Girão [b]

[a] Departamento de Física, Universidade Federal do Ceará, CEP 60455-900, P.O. Box 6030, Fortaleza, Ceará, Brazil
[b] Departamento de Física, Universidade Federal do Piauí, CEP 64049-550, Teresina, Piauí, Brazil
[c] Instituto de Física, Universidade Federal de Uberlândia, CEP 38400-902, Uberlândia, Minas Gerais, Brazil
[d] Department of Physics, Applied Physics, and Astronomy, Rensselaer Polytechnic Institute, Troy, NY, USA

ARTICLE INFO

Article history:
Received 21 August 2017
Received in revised form 17 November 2017
Accepted 20 November 2017
Available online 22 November 2017

Keywords:
Rhombic-GQD
11-AGNR
Molecular electronics
NEGF-DFT
Electron transport

ABSTRACT

Spin-polarized transport through a rhombic graphene quantum dot (rGQD) attached to armchair graphene nanoribbon (AGNR) electrodes is investigated by means of the Green's function technique combined with single-band tight-binding (TB) approach including a Hubbard-like term. The Hubbard repulsion was included within the mean-field approximation. Compared to anti-ferromagnetic (AFM), we show that the ferromagnetic (FM) ordering of the rGQD corresponds to a smaller bandgap, thus resulting in an efficient spin injector. As a consequence, the electron transport spectrum reveals a spin valve effect, which is controlled by doping with B/N atoms creating a *p-n*-type junction. The calculations point out that such systems can be used as spin-filter devices with efficiency close to a 100%.

1. Introduction

Carbon-based molecular devices have attracted increasing attention due to their unique electronic and magnetic properties [1–3]. Compared to metal electrode systems, carbon devices exhibit large electromechanical stability and mechanical flexibility, ensuring greater control over the interface between molecule and electrode[4–7]. Moreover, their long spin-coherence time is desirable for quantum information processing implementations [8,9]. Theoretical[10–12] studies and experimental[13–16] reports have shown that the magnetic properties of a number of graphene-based materials are highly sensitive to their edge geometries. Notably, carbon-based materials with zigzag edges possess magnetic ordering[17,18], while systems with armchair edges do not show any magnetization [19].

The electrical injection of spin-polarized electrons in spintronic devices can be achieved by driving a current from a ferromagnetic (FM) contact [20–22]. With this in mind, a variety of complex devices based on the zigzag graphene nanoribbons (ZGNRs) have been studied [23–26]. It is established that ZGNRs have zero net magnetization ($S = 0$) in their ground state, due to the antiferromagnetic (AFM) coupling between their edges, as predicted by Lieb's theorem [27]. In order to explore the spin degree of freedom of the carriers in those structures, ZGNRs can be tuned from AFM to FM configuration using different approaches, such as chemical substitution on the H-terminated edges [28,29], B and N doping [30–32], topological defects, application of a transversal electric field [33,34], or by exploiting spin–orbit coupling effects [35]. In particular, studies in nano-graphene sandwich-like structure pointed that the exchange coupling, the anisotropy, and the external magnetic field possess an important role on the magnetic properties for the nanographene structure [36,37].

Another class of graphene based structures which also show relevant magnetic configurations in their ground state are graphene quantum dots (GQDs), which are nanometer-sized planar fragments of graphene. Especially, GQDs present the photo-induced electron transfer property, which might be used to increase efficiency of solar cells and optoelectronics components [38–41]. Several studies have been carried out to investigate the electronic and magnetic properties for different shaped GQDs [42–45]. The magnetization of GQDs, present in the case of an unequal number of interpenetrating A and B sublattices (Lieb's theorem [27]), is exploited in many devices with intriguing physical properties, such as long-range electron tunneling [46,47], current switching [48,49], field-effect characteristics [50,51], current rectification [52–54], and spin filter effect [55,56].

In this paper, we report a theoretical study of the electronic structure and spin-polarized transport properties in a two-probe system consisting of a rhombic GQD (rGQD) sandwiched between nonmagnetic armchair graphene nanoribbons (AGNRs) electrodes.

* Corresponding author.
E-mail addresses: aldi@ufpi.edu.br (A. Saraiva-Souza), edu@ufpi.edu.br (E.C. Girão).

https://doi.org/10.1016/j.jmmm.2017.11.089
0304-8853/

In order to explore the magnetic properties of the isolated rGQD, we examine this structure with different magnetic configurations. Despite their different electronic bandgaps, the frontier orbital states possess distinct characteristics. In particular, the ferromagnetic ordering has a smaller bandgap and it is more suitable to be used as an efficient spin injector. Based on this configuration, spin-dependent transport is observed. More importantly, a nearly perfect spin filter effect is found considering different substitutional dopants (B and N atoms). Doping gives rise to a semiconductor-to-metal transition accompanied by substantial changes of the spin-dependent transmission spectra, thus suggesting the possibility of their use as spin-filter devices with an efficiency close to 100%.

2. Theoretical model

We investigate the spin-polarized transport in a two-probe system as illustrated in Fig. 1. The central region includes a rGQD which is coupled to two semi-infinite 11-AGNR electrodes which extend to the left and right directions of the scattering region. In order to keep smooth electronic charge between the electrodes and the central region, seven buffer layers are included in the central region. We investigate two configurations which differ from each other by the type of doping d_1 and d_2 on the left and right leads, respectively (see Fig. 1). As the graphene honeycomb lattice is composed by two interpenetrating triangular sub-lattices A and B, the doping atoms are located in the same C–C dimer line from the AGNRs, but on different sublattices (A = d_1 and B = d_2). The configurations are identified as I ($d_1 = d_2$ = C, undoped) and II (d_1 = B and d_2 = N, doped) systems.

The Hamiltonian describing the system sketched in Fig. 1 is written as $\mathbf{H} = \mathbf{H}_0 + \mathbf{H}'$, where $\mathbf{H}_0$ is the usual tight-binding Hamiltonian given by

$$\mathbf{H}_0 = \sum_{j,\sigma} \epsilon_j |j,\sigma\rangle\langle j,\sigma| + \sum_{i,j,\sigma} \gamma_{ji} |j,\sigma\rangle\langle i,\sigma|, \tag{1}$$

where $|j,\sigma\rangle$ stands for the atomic orbital with spin σ centered on atom j. Here the Hamiltonian is restricted to the π-orbitals from the C, B, and N atoms. ϵ_j and γ_{ji} are the on-site energy and hopping integrals, respectively. Those parameters adopt an appropriate parametrization which includes carbon–carbon interactions up to third-nearest-neighbors [57]. For simplicity, we set carbon-boron and carbon–nitrogen hopping integrals as being the same as those for carbon–carbon interactions, while on-site energies are set either above (B-doping case) or below (N-doping case) carbon's site energy. These ϵ_B and ϵ_N values relative to $\epsilon_C = 0$ are chosen to be similar to renormalized on-site energies proposed for the study of N and B doping on carbon nanotubes [58]. Such choice results in bandstructures for B and N doped AGNRs in good agreement with DFT results [30].

The Coulomb interaction written in the atomic orbital basis can be cast in the Hubbard term in a mean-field fashion as

$$\mathbf{H}\prime = U\sum_j \left(\langle \hat{n}_j^{\uparrow} \rangle \hat{n}_j^{\downarrow} + \langle \hat{n}_j^{\downarrow} \rangle \hat{n}_j^{\uparrow} \right), \tag{2}$$

where $\langle \hat{n}_j^{\sigma} \rangle$ is the average occupation for site j, $\hat{n}_j^{\sigma}$ is the number operator, and $\sigma = \uparrow, \downarrow$ is the spin component. The parameter U is the on-site Coulomb repulsion strength for which we used $U = 2.944$ eV as proposed earlier [59]. From the theoretical point of view, the value of U cannot be directly compared to different simulation methods. However, it is possible to compare the dimensionless parameter U/γ, where γ is the first nearest neighbor interaction term [60]. Results from DFT calculations performed using local-spin-density approximation are best reproduced when $U/\gamma = 0.9$ [17,18]. Therefore, we choose an optimal value of U that corresponds to $U/\gamma = 0.92$. Moreover, quantum Monte Carlo simulations correctly described the honeycomb lattice of graphene with U/γ ranging from 0.9 to 1.3 [61]. On the other hand, magnetic resonance studies of neutral soliton states in trans-polyacetylene gives U values between ≈3.0 and 3.5 eV [62,63].

For the electronic transport calculations, we used a combination of the Landauer formalism [64] and the Green's function technique [65]. Landauer's formula relates quantum conductance $\mathcal{G}$ with transmission spectrum T through

$$\mathcal{G} = \frac{e^2}{h} T. \tag{3}$$

Transmission is computed through the Green's function approach. The retarded/advanced Green's function is given by

$$\mathbf{G}^{r,a} = [E\mathbf{I} \pm i\eta - \mathbf{H} - \Sigma_L(E) - \Sigma_R(E)]^{-1}, \tag{4}$$

where $\Sigma_{L,R}$ are self-energy matrices which are obtained through an iterative procedure [66,67] and the computation of $\mathbf{G}^{r,a}$ is made by means of a set of iterative algorithms [68,69]. The η quantity is a small energy term ($= 10^{-6}$ eV) used to ensure causality in the calculation of $\Sigma_{L,R}$. The transmission coefficient is obtained from the standard result [65]

$$T_\sigma(E) = \mathrm{Tr}[\Gamma_L \mathbf{G}^r \Gamma_R \mathbf{G}^a], \tag{5}$$

where the coupling matrix $\Gamma_{(L/R)}$ is found via the self-energy according to

$$\Gamma_{(L/R)} = i[\Sigma_{(L/R)}(E) - \Sigma^{\dagger}_{(L/R)}(E)]. \tag{6}$$

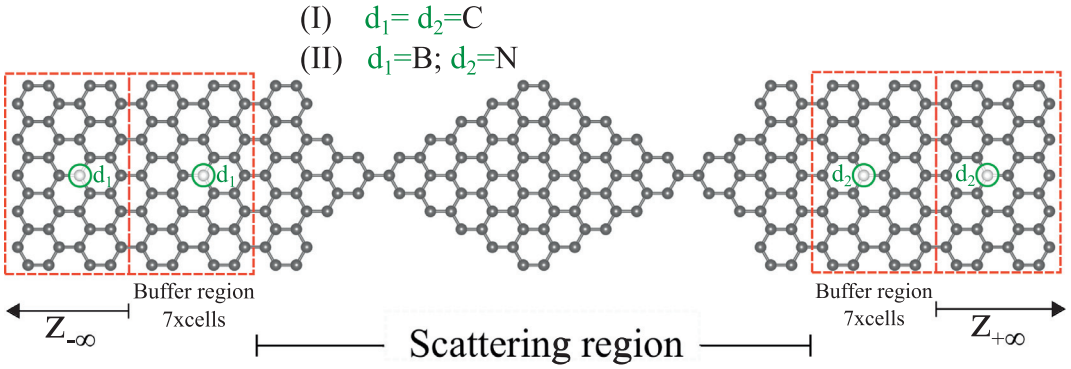

Fig. 1. Schematic representation of AGNR/rGNF/AGNR two-probe system. Dopant positions d_1 and d_2 are distinguished by marked atoms in the left ($z_{-\infty}$) and right ($z_{+\infty}$) region at different sublattices. The configuration I corresponds to $d_1 = d_2$ = C and II to d_1 = B and d_2 = N, representing the undoped and doped systems, respectively. The C atoms are colored in gray and the dopant in white.